

Scalp-Implantable MIMO Antenna for High-Data-Rate Head Implants

Amjad Iqbal, *Member, IEEE*, Muath Al-Hasan, *Senior Member, IEEE*, Ismail Ben Mabrouk, *Senior Member, IEEE*, and Mourad Nedil, *Senior Member, IEEE*

Abstract—A quad-element multiple-input multiple-output (MIMO) antenna is designed at 433 MHz Industrial, Scientific, and Medical (ISM) band, to increase the transmission data-rate and minimize the multipath fading. The proposed MIMO antenna consists of semi-circular meandered radiators with a shared ground. It is designed and optimized inside an implantable medical device (IMD) in a human head model. The antenna's results show a 10-dB fractional bandwidth (FBW) of 38.26% (355–523 MHz) with a peak realized gain of -28.3 dBi. A high isolation (> 32.6 dB) between MIMO elements is obtained using a central metallic via. Specific absorption rate (SAR) and link budget are analyzed to validate the effectiveness of this antenna. The 4×4 MIMO channel parameters are calculated and validated. Furthermore, this antenna provides a channel capacity of 19.9 bps/Hz which is about three times higher than the single-input single-output (SISO) configuration of ≈ 5.89 bps/Hz. Hence, this MIMO configuration is a promising candidate for high-data-rate head implants.

Index Terms—MIMO antenna, implantable medical devices, implantable antenna, coupling coefficient, mutual coupling.

I. INTRODUCTION

RECENTLY, IMDs have gained substantial focus of biomedical engineers due to wide range of applications in medical and healthcare industry [1]-[2]. This is due to the fact that an IMD collects useful information from the user to transfer it to an outside transceiver [3]-[4]. Although an antenna is an important component of an IMD, however, the large space occupied by it is considered as an issue for compact biomedical devices [5]-[6]. Consequently, the IMD's size mainly depends on the antenna's geometry [7]-[8]. Moreover, a reliable communication link with an external receiver is paramount for IMDs [9]-[10]. Therefore, IMDs with low latency and high reliability are desired [11]-[12]. Thus, implantable antennas should have higher gains, stable radiation patterns, and efficient wireless communication links. In fact, designing such antennas inside the human body is still a challenging task due to number of issues, such as biocompatibility, impedance matching, wide bandwidth, size

restriction, human safety, and reliable communication link with an external device [11]-[13].

In this context, several implantable antennas have been suggested using single-input single-output (SISO) configurations [14]. However, current SISO antennas cannot satisfy the needs of modern IMDs due to their limited data-rate and low spectral efficiency [15]. Hence, few MIMO antenna systems have been proposed to solve the problems of SISO configurations. In [16], a dual-port MIMO antenna, based on a spiral resonator and a capacitor, is reported to transfer real-time high-resolution images from capsule endoscope to an external device. It operates at 433 MHz with an FBW of only 3.2% and large dimensions of 120 mm³. In [17], a quad-port meandered antenna, combined with metamaterial, is introduced to maintain high isolation. This antenna has an FBW of 18.64% and occupies large volume of 434.6 mm³. In [18], a spiral resonator is adopted to design a dual-port MIMO antenna at 403 MHz Medical Device Radiocommunication Service (MedRadio) band with an adequate FBW of 35.9% and isolation of 25.6 dB. This antenna occupies large dimensions of 307 mm³. In [19], two-element single band antenna is designed. In this design, metallic vias are used for miniaturization and neutralization line is adopted to increase isolation. Consequently, it operates with an isolation = 37 dB and FBW = 8.5%. In [20]-[21], non-planar implantable MIMO antennas are reported; however, their non-planar and large geometry restricts their applications in compact IMDs. In fact, the majority of the suggested implantable MIMO antennas have large dimensions with narrow bandwidths.

To address the aforementioned limitations, a compact and low profile quad-port implantable antenna is proposed. The compactness is achieved using a semi-circular meandered geometry, while isolation between the elements is enhanced through a central metallic via. Consequently, it has dimensions of 23.69 mm³ and isolation of > 32.6 dB. Furthermore, it has a wide bandwidth of 38.26% (355–523 MHz) and peak realized gain of -28.3 dBi. The advantages of the proposed prototype are 1) compact and low profile, 2) highly uncorrelated MIMO channels, 3) wide operating bandwidth, and 4) high channel capacity.

II. IMPLANTABLE MIMO ANTENNA DESIGN

The geometry of the proposed four-port implantable MIMO antenna is shown in Fig. 1. Each radiator is composed of semi-circular shaped meandered radiator, excited by a 50 Ω coaxial probe. A high dielectric constant laminate RO3010 (ϵ_r ,

This work was supported by the Abu-Dhabi Department of Education and Knowledge (ADEK) Award for Research Excellence 2019 under Grant AARE19-245 (*Corresponding Author: Amjad Iqbal*)

A. Iqbal and I. Ben Mabrouk are with the Department of Engineering, Durham University, Durham DH1 3LE, UK (e-mail: aiqbal@ieee.org, ismail.benmabrouk@durham.ac.uk).

M. Al-Hasan is with the Network and Communications Engineering Department, Al Ain University, Al Ain, United Arab Emirates (e-mail: muath.alhasan@aau.ac.ae).

M. Nedil is with the Communications Research Laboratory (LRTCS), University of Quebec at Abitibi-Temiscamingue (UQAT), Val-d'Or, QC J9P 1Y3, Canada (e-mail: mourad.nedil@uqat.ca).

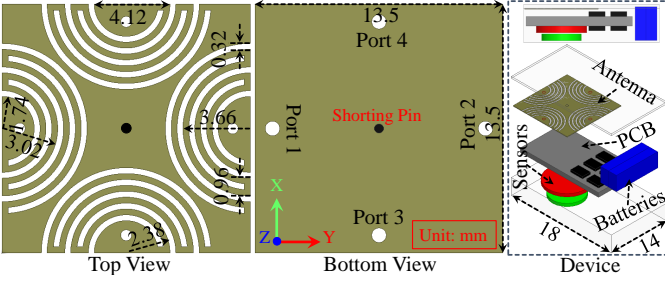


Fig. 1: Geometry of the proposed MIMO antenna and device architecture.

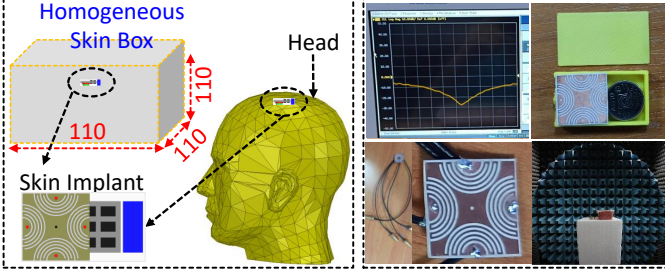


Fig. 2: Simulation environment and measurement setup of the antenna.

$= 10.2$, and $\tan\delta = 0.0022$) is used as a substrate. An ultra-thin laminate (0.13 mm) is chosen as a substrate to minimize the flow of surface waves from one port to another. Hence, mutual coupling is reduced [22]. A metallic via of 0.5 mm diameter is placed at the centre of the antenna to further reduce the flow of surface waves. Accordingly, mutual coupling between the elements is further reduced. The proposed antenna system has compact dimensions of $0.062\lambda_g \times 0.062\lambda_g \times 0.0005\lambda_g$, where λ_g is the guided-wavelength at 433 MHz, and a common ground plane. An implantable antenna is always employed inside an IMD containing radio-frequency (RF) and electronic parts. Since this antenna is designed for head implants, the antenna is designed and optimized inside a flat-type device, as shown in Fig. 1. First, the proposed antenna is investigated in a $110 \times 110 \times 110$ mm³ skin phantom and then in a realistic human head model (Fig. 2). The electric characteristics of the skin phantom has been chosen as $\epsilon_r = 46.08$ and $\sigma = 0.702$ S/m [23]. In both scenarios, the antenna is placed at a depth of 4 mm. It is worth mentioning that all results presented in this work are based on the antenna being implanted in a realistic human head model. All electromagnetic (EM) simulations are performed using High Frequency Structure Simulator (HFSS). The simulated S-parameters of the implantable MIMO antenna system is shown in Fig. 3. It can be seen that this antenna operates at 433 MHz with a simulated FBW of 38.26 %, and isolation of more than 32.6 dB. The presence of some conductive surfaces such as copper pads for capacitors, inductors, capacitors and other surface mounted devices in the vicinity of each antenna elements could affect their impedance matching [10],[24],[25]. In our case, the position of each antenna element is at different distances from the conductive surfaces. Therefore, the impedance matching of all elements are not similar. Moreover, the mutual coupling

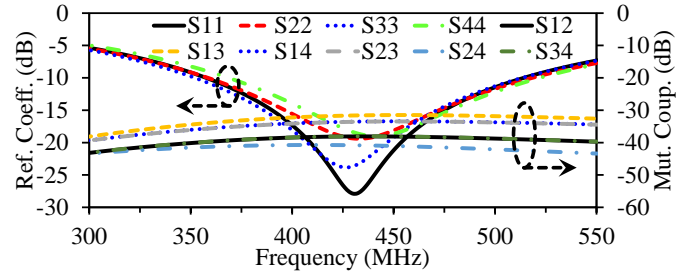


Fig. 3: S-parameters of the proposed MIMO antenna at implantation depth of 4 mm.

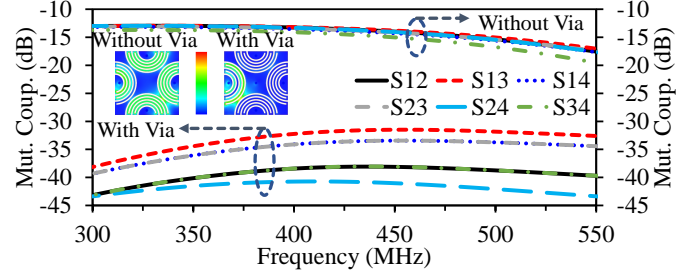


Fig. 4: Mutual coupling and current density with and without metallic via at implantation depth of 4 mm.

between antenna elements depends on the distance between them [26],[27]. Therefore, mutual coupling values are different for each pair of antenna elements.

Several steps have been considered in the design process to achieve compactness and high isolation. Initially, the miniaturization of a square patch antenna is achieved using semi-circular meandered resonators. In fact, the semi-circular meandered resonators increase the current path that shift the resonant frequency to the lower ones. Then, a central metallic via is used to maintain high isolation between MIMO elements. Fig. 4 shows the results (S-parameters and surface current density) of the antenna with and without the central metallic via. It can be observed that the current of the excited element (without via) is highly coupled with passive elements. However, the current is minimally coupled with passive elements in the presence of central via. Similar phenomenon is also observed in terms of mutual coupling results. In fact, decoupling is increased by introducing the central metallic via. More specifically, the isolation level is increased to 32.6 dB from 15 dB through central via (Fig. 4).

The decoupling phenomenon using a central metallic via is further elaborated using equivalent circuit model, as illustrated in Fig. 5. An accurate lumped element model is extracted using Keysight ADS, where all resonators are expressed as a parallel RLC circuit [28]. First, a circuit is designed for a MIMO system without including a central metallic via. The coupling coefficient between the resonators is expressed as K_{12} , K_{13} , K_{14} , K_{23} , K_{24} , and K_{34} . Then, a parallel RLC circuit (central metallic vias) is coupled with four resonators. In this context, K_{1d} expresses the coupling of resonator 1 with the central via; K_{2d} is the coupling of resonator 2 with the central via; K_{3d} is the coupling of resonator 3 with the central via; and K_{4d} is the coupling of resonator 4 with the central via. In fact,

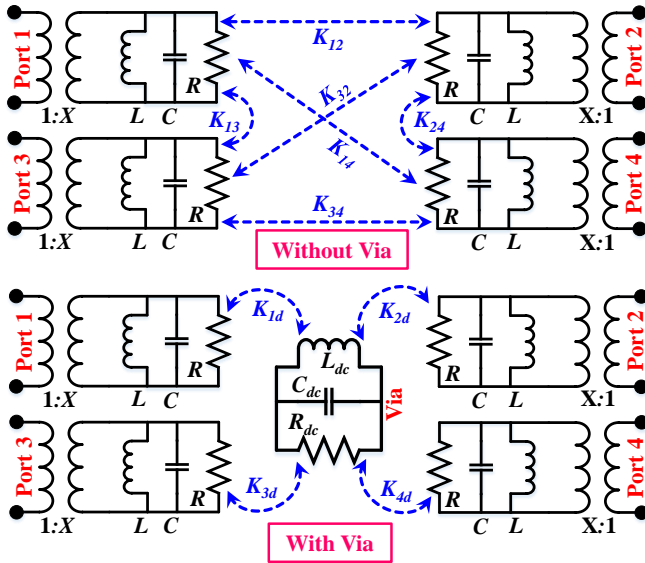


Fig. 5: Equivalent circuit model of quad-element MIMO antenna system ($X = 1.1$, $R = 43.25 \Omega$, $L = 7.68 \text{ nH}$, $C = 16.3 \text{ pF}$, $R_{dc} = 149.3 \Omega$, $L_{dc} = 0.98 \text{ nH}$, $C_{dc} = 4.2 \text{ pF}$, $K_{12} = 0.09$, $K_{13} = 0.10$, $K_{14} = 0.07$, $K_{23} = 0.09$, $K_{24} = 0.08$, $K_{34} = 0.11$, $K_{1d} = 3$, $K_{2d} = 1.38$, $K_{3d} = 2.8$, and $K_{4d} = 1.33$).

all resonators are directly coupled with the decoupling circuit (R_{dc} , L_{dc} , and C_{dc}). Therefore, the coupling level between antenna elements is reduced. Hence, isolation between antenna elements is increased. The optimized circuit values are given in the caption of Fig. 5. The S-parameters of the circuit model are compared with the EM model and the fabricated model, as shown in Fig. 6.

III. RESULTS AND DISCUSSIONS

This antenna is initially designed in a cubical skin phantom to reduce the computational complexity. Later, it is integrated in a flat-type device and optimized inside a realistic human head model. Then, an accurate circuit model is developed to validate the concept. Finally, the antenna is fabricated on the Rogers RO3010 substrate and integrated in a flat-type biocompatible alumina ($\epsilon_r = 9.8$) device, as shown in Fig. 2. Furthermore, 3D printing technology is used to fabricate the casing of the flat-type device. Then, the antenna prototype along with other IMD components are placed inside the device, where the lid is closed using epoxy. Afterwards, the flat-type device is placed inside minced pork meat for practical measurements. The S-parameters measurements are performed by connecting two ports of the antenna to the network analyzer and the rest of the ports are terminated with a 50Ω load. The measured S_{11} has the resonance at 435 MHz with a 10-dB bandwidth of 40.35% (356-536 MHz) and isolation (S_{21}) of more than 37 dB, as shown in Fig. 6. The radiation patterns and gain of the antenna at 433 MHz are also measured. While measuring the radiation patterns, only one port is attached to the analyzer and all others are terminated with a 50Ω load. A high-gain horn antenna is used as a transmitting antenna and is placed 3 meters away from the proposed antenna. The horn

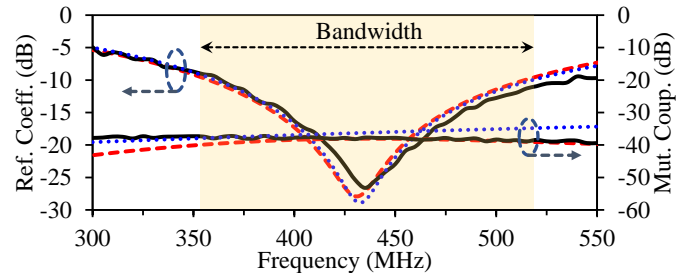


Fig. 6: S-parameters of the EM model (dashed line), equivalent circuit model (dotted line), and fabricated prototype (solid line).

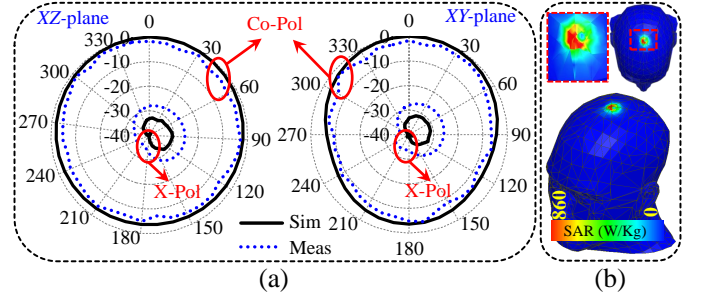


Fig. 7: (a) Normalized radiation patterns (XZ- and YZ-plane) of the antenna at 433 MHz. (b) 10-g SAR at 433 MHz for 1 W input power.

antenna has a width = 49 cm, height = 32 cm and depth = 40 cm. It can be observed from Fig. 7a that the proposed antenna has nearly omni-directional radiation pattern. It is worth mentioning that omni-directional radiation patterns are highly desired for biomedical implants due to their ability to transmit and receive signal from all directions. At 433 MHz, the simulated and measured peak realized gain of the antenna is -28.3 dBi and -30.1 dBi , respectively. Moreover, it has a radiation efficiency of -34.5 dB at 433 MHz.

Input power and specific absorption rate (SAR) are important factors to ensure human safety. In fact, peak SAR value should be lower than 2 W/kg (averaged over a 10-g of tissue) for an input power of 1 W. When all antenna's elements are excited with 1 W of input power, a peak SAR value of 860 W/Kg is observed, as illustrated in Fig. 7b. In fact, each element of the antenna contributes 215 W/Kg to the total SAR value. According to IEEE C95.1-2019, the proposed antenna can support input power up to 9.3 mW for a safe operation. In practical applications, a maximum power of -16 dBm (ITU-R RS.1346) is allowed for implants to avoid interference with other devices [24]. Therefore, the proposed antenna is even safe for an input power of 9.68 dBm (9.3 mW).

Moreover, a robust communication link is important to exchange the information between the implant and external device. Therefore, a link margin ($\text{LM [dB]} = P_a - P_r$) is calculated based on Equations (1)-(2) [17]. The link margin is calculated using different data-rates at 433 MHz, as illustrated in Fig. 8. Considering at least 20 dB link margin, the proposed implantable MIMO antenna can successfully transmit the data over 25 meters at 78 Mbps.

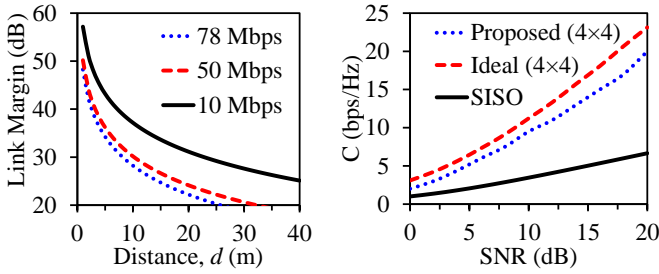


Fig. 8: Calculated link margins and channel capacities.

$$P_a[dB] = P_t + G_t + G_r - 10\log_{10}(4\pi d/\lambda)^2 - N_o \quad (1)$$

$$P_r[dB] = E_b/N_o + 10\log_{10}(B_r) + G_d \quad (2)$$

where, $P_t = -16$ dBm is the transmitted power, $G_t = -28.3$ dBi is the transmitting antenna gain, $G_r = 2$ dBi is the receiving antenna gain, λ is the wavelength at 433 MHz, d is the distance between the receiving and transmitting antennas, $N_o = -199.5$ dB/Hz is the noise power density, $E_b/N_o = 9.6$ dB is the ideal PSK, B_r is the bit rate, and $G_d = 2.5$ dB is the fixing deterioration.

A. MIMO Channel Parameters

The main advantage of the MIMO antenna is its high channel capacity without additional bandwidth and power. Ideally, the channel capacity of the uncorrelated MIMO system increases with more antennas. But in practical applications, one cannot achieve uncorrelated channels. The channel capacity of $N \times N$ MIMO antenna system is calculated using Equation (3) [29].

$$CC = \log_2(\det[I + (SNR/N)HH^*]) \quad (3)$$

where CC is the channel capacity, SNR expresses the signal to noise ratio, H is the channel matrix and is calculated from the radiation patterns of the antenna, I is the identity matrix, and H^* is the conjugate of H matrix. In fact, H matrix contains the gain and phase information of MIMO elements. The channel matrix (H) is calculated using standard equations of [30], [31]. The calculated channel capacity as a function of SNR values is shown in Fig. 8. It can be observed that the channel capacity of the proposed MIMO antenna is higher than SISO configuration under similar conditions. Considering $SNR = 20$ dB, the proposed antenna has channel capacity of 19.9 bps/Hz; which is almost three times higher than the SISO configuration of ≈ 5.89 bps/Hz [32]. Hence, this antenna is a promising candidate for high-data-rate head implants.

The Envelop Correlation Coefficient (ECC) is a vital MIMO channel parameter, which characterizes the dependency of MIMO elements. The ECC of the MIMO antenna system can be determined from S-parameters [33] or far-fields [34]-[35]. In our study, far-field patterns are used to calculate the ECC [35]. In fact, $ECC < 0.5$ is considered as a fair value for high channel capacity [36]. It can be observed from Fig. 9 that the ECC values are less than 0.1 in the overall frequency band.

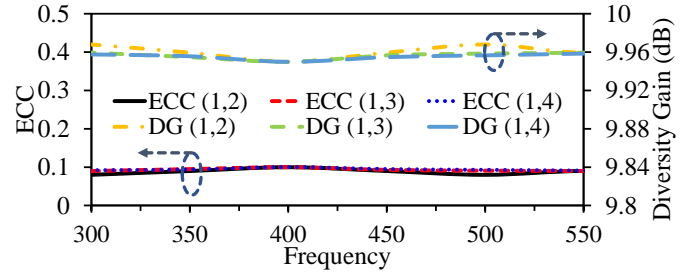


Fig. 9: Simulated ECC and DG of the implantable MIMO antenna system.

TABLE I: Comparison of the proposed implantable MIMO antenna with other implantable MIMO antennas.

Ref.	[16]	[17]	[18]	[19]	[20]	[21]	Proposed
Size (mm ³)	120	434.6	307.3	280	3375	2879	23.6
Size (λ_g^3)	0.00002	0.003	0.000009	0.002	0.004	0.004	0.000019
Tissue Layers	1	3	1	3	3	1	Head model
Elements	2	4	2	2	4	2	4
Freq. (GHz)	0.433	2.45	0.402	2.45	2.45, 5.8	2.46	0.433
BW (%)	3.2	18.64	35.9	8.5	36, 26	14.1	38.26
Isolation (dB)	12.17	15.9	25.6	37	32	30	32.6
ECC	NR	0.002	NR	NR	0.1	NR	0.1
DG (dB)	NR	NR	NR	NR	NR	NR	9.95
CC (bps/Hz)	NR	NR	NR	NR	NR	NR	19.9@SNR = 20 dB

BW: Bandwidth, Freq.: Frequency, NR: Not reported, SLS: System level study

Similarly, the Diversity Gain (DG) is another important parameter to assess a MIMO system, which has an inverse relationship with the ECC. A DG of 10 dB is expected for completely uncorrelated MIMO channels. The DG of the proposed MIMO antenna system is calculated using equation [37]. The calculated DG of the antenna is higher than 9.95 dB in the entire operating band, as shown in Fig. 9.

In Table I, the performance of the proposed implantable MIMO antenna is compared with state-of-the-art implantable MIMO antennas. It can be observed that the proposed antenna has larger bandwidth and smaller dimensions compared to other implantable antennas. Furthermore, it has higher isolation than majority of the antennas. Moreover, important channel parameters, such as diversity gain and channel capacities are not fully reported in the previous studies.

IV. CONCLUSION

A compact and wideband quad-element MIMO antenna is developed for high-data-rate head implants. The MIMO antenna operates at 433 MHz ISM band with a 10-dB wide bandwidth of 38.26 % (355–523 MHz) and port isolation of more than 32.6 dB. The compact dimensions of $13.5 \times 13.5 \times 0.13$ mm³ ($0.062\lambda_g \times 0.062\lambda_g \times 0.0005\lambda_g$) are achieved using a semi-circular meandered geometry, while isolation is enhanced through the central metallic via. This antenna is validated, considering it in a flat-device, in a realistic human head model, and minced pork meat. The MIMO channel parameters such as ECC, DG, and channel capacity are calculated which show promising results.

REFERENCES

- [1] D. Panescu, "Emerging technologies [wireless communication systems for implantable medical devices]," *IEEE Engineering in Medicine and Biology Magazine*, vol. 27, no. 2, pp. 96–101, 2008.
- [2] T. Karacolak, A. Z. Hood, and E. Topsakal, "Design of a dual-band implantable antenna and development of skin mimicking gels for continuous glucose monitoring," *IEEE Transactions on Microwave Theory and Techniques*, vol. 56, no. 4, pp. 1001–1008, 2008.
- [3] Z. Bao, Y.-X. Guo, and R. Mittra, "Single-layer dual/tri-band inverted-f antennas for conformal capsule type of applications," *IEEE Transactions on Antennas and Propagation*, vol. 65, no. 12, pp. 7257–7265, 2017.
- [4] B. Biswas, A. Karmakar, and V. Chandra, "Miniaturised wideband ingestible antenna for wireless capsule endoscopy," *IET Microwaves, Antennas & Propagation*, vol. 14, no. 4, pp. 293–301, 2019.
- [5] A. Iqbal, M. Al-Hasan, I. B. Mabrouk, A. Basir, M. Nedil, and H. Yoo, "Biotelemetry and wireless powering of biomedical implants using a rectifier integrated self-diplexing implantable antenna," *IEEE Transactions on Microwave Theory and Techniques*, vol. 69, no. 7, pp. 3438–3451, 2021.
- [6] C. Liu, Y.-X. Guo, and S. Xiao, "Capacitively loaded circularly polarized implantable patch antenna for ism band biomedical applications," *IEEE transactions on antennas and propagation*, vol. 62, no. 5, pp. 2407–2417, 2014.
- [7] D. Nikolayev, M. Zhadobov, L. Le Coq, P. Karban, and R. Sauleau, "Robust ultraminiature capsule antenna for ingestible and implantable applications," *IEEE Transactions on Antennas and Propagation*, vol. 65, no. 11, pp. 6107–6119, 2017.
- [8] C. Liu, Y. Zhang, and X. Liu, "Circularly polarized implantable antenna for 915 mhz ism-band far-field wireless power transmission," *IEEE Antennas and Wireless Propagation Letters*, vol. 17, no. 3, pp. 373–376, 2018.
- [9] S. M. Asif, A. Iftikhar, B. D. Braaten, D. L. Ewert, and K. Maile, "A wide-band tissue numerical model for deeply implantable antennas for rf-powered leadless pacemakers," *IEEE Access*, vol. 7, pp. 31 031–31 042, 2019.
- [10] S. A. A. Shah and H. Yoo, "Scalp-implantable antenna systems for intracranial pressure monitoring," *IEEE Transactions on Antennas and Propagation*, vol. 66, no. 4, pp. 2170–2173, 2018.
- [11] A. Kiourti and K. S. Nikita, "A review of implantable patch antennas for biomedical telemetry: Challenges and solutions [wireless corner]," *IEEE Antennas and Propagation Magazine*, vol. 54, no. 3, pp. 210–228, 2012.
- [12] F. Merli, L. Bolomey, J.-F. Zurcher, G. Corradini, E. Meurville, and A. K. Skrivervik, "Design, realization and measurements of a miniature antenna for implantable wireless communication systems," *IEEE Transactions on Antennas and propagation*, vol. 59, no. 10, pp. 3544–3555, 2011.
- [13] T.-A. Le Trong, S. I. H. Shah, G. Shin, S. M. Radha, and I.-J. Yoon, "A compact triple-band antenna with a broadside radiation characteristic for head-implantable wireless communications," *IEEE Antennas and Wireless Propagation Letters*, vol. 20, no. 6, pp. 958–962, 2021.
- [14] M. Al-Hasan, P. R. Sura, A. Iqbal, J. J. Tiang, I. B. Mabrouk, and M. Nedil, "Low-profile dual-band implantable antenna for compact implantable biomedical devices," *AEU-International Journal of Electronics and Communications*, vol. 138, p. 153896, 2021.
- [15] A. Iqbal, M. Al-Hasan, I. B. Mabrouk, and M. Nedil, "A compact implantable mimo antenna for high data rate biotelemetry applications," *IEEE Transactions on Antennas and Propagation*, 2021.
- [16] P. L. Poshtgol, L. Jichao, S. Soltani, and R. D. Murch, "Mimo antennas for capsule endoscope systems," in *2016 IEEE International Symposium on Antennas and Propagation (APSURSI)*. IEEE, 2016, pp. 1175–1176.
- [17] Y. Fan, J. Huang, T. Chang, and X. Liu, "A miniaturized four-element mimo antenna with ebg for implantable medical devices," *IEEE Journal of Electromagnetics, RF and Microwaves in Medicine and Biology*, vol. 2, no. 4, pp. 226–233, 2018.
- [18] S. Xiao, C. Liu, Y. Li, X. M. Yang, and X. Liu, "Small-size dual-antenna implantable system for biotelemetry devices," *IEEE Antennas and Wireless Propagation Letters*, vol. 15, pp. 1723–1726, 2016.
- [19] S. S. Moirangthem, J. Ghosh, S. Ghosh, and A. Sarkhel, "Miniaturized dual antenna system for implantable bio-telemetry application," *IEEE Antennas and Wireless Propagation Letters*, pp. 1–1, 2021.
- [20] V. Kaim, B. K. Kanaujia, and K. Rambabu, "Quadrilateral spatial diversity circularly polarized mimo cubic implantable antenna system for biotelemetry," *IEEE Transactions on Antennas and Propagation*, vol. 69, no. 3, pp. 1260–1272, 2021.
- [21] L. Matekovits, J. Huang, I. Peter, and K. P. Esselle, "Mutual coupling reduction between implanted microstrip antennas on a cylindrical bi-metallic ground plane," *IEEE Access*, vol. 5, pp. 8804–8811, 2017.
- [22] A. Iqbal, A. Basir, A. Smida, N. K. Mallat, I. Elfergani, J. Rodriguez, and S. Kim, "Electromagnetic bandgap backed millimeter-wave mimo antenna for wearable applications," *IEEE Access*, vol. 7, pp. 111 135–111 144, 2019.
- [23] D. Miklavčič, N. Pavšelj, and F. X. Hart, "Electric properties of tissues," *Wiley encyclopedia of biomedical engineering*, 2006.
- [24] A. Basir and H. Yoo, "A stable impedance-matched ultrawideband antenna system mitigating detuning effects for multiple biotelemetric applications," *IEEE Transactions on Antennas and Propagation*, vol. 67, no. 5, pp. 3416–3421, 2019.
- [25] S. A. A. Shah and H. Yoo, "Radiative near-field wireless power transfer to scalp-implantable biotelemetric device," *IEEE Transactions on Microwave Theory and Techniques*, vol. 68, no. 7, pp. 2944–2953, 2020.
- [26] I. Nadeem and D.-Y. Choi, "Study on mutual coupling reduction technique for mimo antennas," *IEEE Access*, vol. 7, pp. 563–586, 2018.
- [27] A. Iqbal, O. A. Saraereh, A. W. Ahmad, and S. Bashir, "Mutual coupling reduction using f-shaped stubs in uwb-mimo antenna," *IEEE Access*, vol. 6, pp. 2755–2759, 2017.
- [28] Z. Qamar, U. Naeem, S. A. Khan, M. Chongcheawchamnan, and M. F. Shafique, "Mutual coupling reduction for high-performance densely packed patch antenna arrays on finite substrate," *IEEE Transactions on Antennas and Propagation*, vol. 64, no. 5, pp. 1653–1660, 2016.
- [29] D. Gesbert, M. Shafi, D. shan Shiu, P. Smith, and A. Naguib, "From theory to practice: an overview of mimo space-time coded wireless systems," *IEEE Journal on Selected Areas in Communications*, vol. 21, no. 3, pp. 281–302, 2003.
- [30] P.-S. Kildal and K. Rosengren, "Correlation and capacity of mimo systems and mutual coupling, radiation efficiency, and diversity gain of their antennas: simulations and measurements in a reverberation chamber," *IEEE Communications Magazine*, vol. 42, no. 12, pp. 104–112, 2004.
- [31] Z. Li, Z. Du, M. Takahashi, K. Saito, and K. Ito, "Reducing mutual coupling of mimo antennas with parasitic elements for mobile terminals," *IEEE Transactions on Antennas and Propagation*, vol. 60, no. 2, pp. 473–481, 2012.
- [32] E. Ghayoula, A. Bouallegue, R. Ghayoula, and J. Chouinard, "Capacity and performance of mimo systems for wireless communications," *Journal of Engineering Science and Technology, Review*, vol. 7, no. 3, 2014.
- [33] A. Iqbal, A. Smida, A. J. Alazemi, M. I. Waly, N. K. Mallat, and S. Kim, "Wideband circularly polarized mimo antenna for high data wearable biotelemetric devices," *IEEE Access*, vol. 8, pp. 17935–17944, 2020.
- [34] M. S. Sharawi, "Current misuses and future prospects for printed multiple-input, multiple-output antenna systems [wireless corner]," *IEEE Antennas and Propagation Magazine*, vol. 59, no. 2, pp. 162–170, 2017.
- [35] J.-F. Qian, F.-C. Chen, Y.-H. Ding, H.-T. Hu, and Q.-X. Chu, "A wide stopband filtering patch antenna and its application in mimo system," *IEEE Transactions on Antennas and Propagation*, vol. 67, no. 1, pp. 654–658, 2018.
- [36] J. Acharjee, K. Mandal, and S. K. Mandal, "Reduction of mutual coupling and cross-polarization of a mimo/diversity antenna using a string of h-shaped dgs," *AEU-International Journal of Electronics and Communications*, vol. 97, pp. 110–119, 2018.
- [37] K. Rosengren and P.-S. Kildal, "Radiation efficiency, correlation, diversity gain and capacity of a six-monopole antenna array for a mimo system: theory, simulation and measurement in reverberation chamber," *IEE Proceedings-Microwaves, Antennas and Propagation*, vol. 152, no. 1, pp. 7–16, 2005.